Highlights

SMART-PIPEBOT: A Soft Pipe-Climbing Robot with Woodpecker Tail-Inspired Support Mechanism for Single-Sidewall Adhesion

Sheng Lin, Gen Li, Ziwei Wang, Jialu Feng, Bo Xiao, Eric M. Yeatman

- Woodpecker-tail-inspired elastic support enables single-sidewall adhesion in large pipes, eliminating multi-point contact.
- Simplified actuation: A single pneumatic unit enables climbing at 0.05 MPa.
- Adapts to large pipes with stable climbing, even on wet walls.
- Flexible adhesion minimizes pipe-wall damage vs. rigid robots.

SMART-PIPEBOT: A Soft Pipe-Climbing Robot with Woodpecker Tail-Inspired Support Mechanism for Single-Sidewall Adhesion

Sheng Lin[a], Gen Li[a], Ziwei Wang[b,*], Jialu Feng[a], Bo Xiao[c] and Eric M. Yeatman[d]

[a]School of Mechanical Engineering, Dalian Jiaotong University, Dalian, 116028, China
[b]School of Engineering, Lancaster University, Lancaster, LA1 4YW, United Kingdom
[c]School of Robotics, Xi'an Jiaotong-Liverpool University, Suzhou, 215000, China
[d]Department of Electrical and Electronic Engineering, Imperial College London, London, SW7 2AZ, United Kingdom

ARTICLE INFO

Keywords:
Soft Robots
Pipeline Climbing Robots
Bio-inspired Design
Pneumatic Adsorption

ABSTRACT

Soft crawling robots have attracted substantial attention for their environmental adaptability and compliant locomotion. However, the scalability of many soft in-pipe robots to large diameters remains limited because their locomotion typically relies on multi-point contact with the pipe inner wall. To overcome this limitation, we propose SMART-PIPEBOT, a woodpecker-tail-inspired adhesion-driven soft pipeline climbing robot that achieves single-sidewall attachment and locomotion in large-diameter pipes while markedly reducing dependence on distributed wall support. SMART-PIPEBOT integrates an inflatable silicone bladder, vacuum sucker brackets, silicone vacuum suckers, a constraining layer, and an elastic tail-support frame. Experiments quantified how vacuum-sucker inclination (10°–50°) affects adhesion at 0.05 MPa and evaluated single-sidewall climbing performance in large-diameter pipes (170, 200, and 230 mm). The maximum mean adhesion force was 26.778 N at a 30° inclination. SMART-PIPEBOT achieves maximum climbing speeds of 16.93 mm/s horizontally and 12.63 mm/s vertically under dry conditions and maintains continuous locomotion on wet walls with mean speeds of 4 mm/s (23.6% of the dry horizontal) and 2 mm/s (15.7% of the dry vertical). Payload experiments further demonstrate a pronounced improvement in effective load capacity when inspection equipment is mounted at the rear rather than the front, enabling a twofold increase in horizontal payload (100 g vs. 50 g) and a 1.5× increase in vertical payload (30 g vs. 20 g).

1. Introduction

Pipelines are critical infrastructure for energy and material transport, and their integrity is central to operational safety, where pipeline integrity management constitutes the core safeguard [1]. However, during prolonged service, pipeline structures inevitably suffer degradation from concurrent factors, including material aging, corrosion effects, and internal pressure fluctuations, leading to structural compromise and potential leakage risks [2, 3]. Consequently, regular pipeline inspections are indispensable for early risk identification and prevention. Traditional manual inspection methods incur substantial human resources and economic costs. This underscores the imperative and urgent necessity to deploy efficient, intelligent inspection robots for enhancing pipeline detection automation levels.

Diverse robotic solutions have been developed to navigate complex pipeline environments. Permanent-magnet-based climbing platforms have been proposed for ferromagnetic pipes, enabling reliable adhesion during vertical, lateral, and elbow traversal [4, 5]. One representative design adopts a modular architecture with omnidirectional wheels, achieving stable motion in straight sections as well as 90° elbows [4], while another enhances adhesion through circumferentially embedded magnets combined with multi-link structures and fuzzy-logic control for obstacle negotiation [5]. Diameter-adaptive mechanisms employing elastic telescopic structures or pneumatic expansion have also been introduced to maintain wall-pressing support across varying pipe sizes [6, 7, 8, 9]. These designs typically use spring-loaded wheels or tracked units to sustain traction, with specific implementations including spiral-angle adjustment for optimized contact force [6], a three-arm half-umbrella support configuration [7], and elastic telescopic linkage systems [8]; in addition, pneumatic actuation has been used to achieve large deformations (up to 191.4%) for obstacle avoidance [9]. To address mobility challenges in bends, non-symmetric wheel layouts (120°/104.88°/135.12°) have been introduced to eliminate motion singularities and maintain uniform contact forces in elbows [10]. Further improvements in maneuverability have been realized through three-section robots with active joints and scissor-leg caterpillar tracks, enabling adaptive yaw and roll for traversing gaps and complex obstacles [11]. For large-diameter pipes (900–1200 mm), inspection systems integrating rotating magnetic flux leakage sensor modules with multiple motorized lifting units have been developed to actively center the robot and maintain wall contact during long-range (>1 km) spiral inspections [12]. Beyond conventional configurations, caterpillar-based robots equipped with contact sensor modules have demonstrated autonomous navigation in 0.5 m diameter pipes, including miter bends and real-time 3D mapping [13]. Multi-gait snake-like robots employing conical spiral motion have also been proposed for compliant inner-wall inspection in 200-500 mm pipes, where optimized backbone curve control is used to reduce mechanical stress on the pipe wall [14]. Existing rigid-configuration pipeline robots based on these principles have successfully achieved locomotion and

*Corresponding author. z.wang82@lancaster.ac.uk
ORCID(s): 0000-0003-4588-8501 (Z. Wang)

climbing functions, but their diameter adaptability remains limited. Moreover, they typically exhibit excessive weight, restricted flexibility in high-curvature pipelines, and a risk of mechanical damage to pipe walls, while their stability predominantly relies on multi-point support structures; magnetic-adhesion-based designs additionally suffer from constraints related to pipe material compatibility. Recently, soft robotics technology has emerged as a promising approach to overcoming these limitations.

Soft pipe-crawling robots utilize diverse anchoring and locomotion strategies. Radial expansion mechanisms dominate wall support, employing hollow shell-lattice structures with opposite deformations [15]; inflatable tentacles with silicone pads [16]; lantern-shaped origami feet [17]; silicone-rubber holding tubes [18]; bellows/grip units with artificial muscles [19]; and dedicated radially expanding pneumatic actuators generating >100 N force for variable diameters (50 - 138 mm), wet or oily surfaces, bends, and payload carriage (up to 30 × weight) [20, 21]. Inchworm-inspired designs often combine radial anchoring with axial movement using modular pneumatic actuators, enabling bend negotiation (90° - 108°) [16, 22, 23, 18]. Specific variants include layer-interference variable stiffness [22], SMA-actuated telescopic modules with braided mesh tubes [24], and micro-control sequences [18]. Magnetically powered versions offer untethered multi-modal locomotion [25]. Dielectric Elastomer Actuator-based robots achieve high speeds (>1 BL/s) using voltage-controlled mechanisms: smart composite microstructure anchors dynamically adjust friction [26], while spring-rolling designs with compliant bristles exploit anisotropic friction (undersized pipes) or bending-moment propulsion (oversize pipes/ground), reaching 3.52 BL/s [27]. Bio-inspired alternatives include: a drosophila larvae robot using obliquely arranged SMA coils and bistable beams for multi-modal motion (twisting/rolling) and valve operation [28]; a rigid-soft snake robot leveraging anisotropic friction from radial pneumatic muscles during wave gaits [29]; and peristaltic robots with endoskeleton springs amplifying force (propulsion 60.2 N, traction 538.9 N) [19]. Unique locomotion mechanisms include: McKibben actuator-triggered elastic ribbon buckling creating anisotropic friction via radially buckling TPU ribbons [30]; enhanced linear antagonistic mechanisms actively boosting traction (268.1 N) for bend navigation [31]; and onboard pneumatic/electrical systems enabling autonomy [20]. Integrated inspection capabilities feature self-powered T-TENG sensors for 99% accurate material recognition in darkness [17] and micro-cameras for real-time viewing [26]. Designs ensure operation in dynamic fluids without flow obstruction [15, 16]. Overall, soft robots leverage their exceptional flexibility to demonstrate distinct strengths in pipe climbing applications [32, 33]. Some draw inspiration from nature through bio-inspired designs, employing soft materials in multi-morphological and multi-structured forms, resulting in robots exhibiting outstanding performance in pipe climbing. However, existing soft robots predominantly rely on comprehensive or multi-point contact with the pipe wall to provide essential support and propulsive reaction force [33, 34]. In large-diameter pipes, achieving sufficient support often requires scaling the robot structure, which increases size and mass and reduces compliance. This inevitably leads to increased bulkiness, reduced flexibility, significantly higher driving energy consumption, diminished passage capability, and may even exceed the load-bearing limits of the materials or driving components.

To address these challenges, we propose a novel soft pneumatic adsorption-based pipe-climbing robot (SMART-PIPEBOT) inspired by the woodpecker tail support mechanism, achieving rapid prototyping, single-sidewall adhesion, and stable vertical climbing capability. The main contribution is an elastic tail-support frame that mimics woodpecker tail-foot synergy [35] to stabilize single-sidewall adhesion. SMART-PIPEBOT comprises an inflatable bladder, vacuum sucker brackets, silicone vacuum suckers, a constraining layer, and an elastic tail support frame, which are manufactured using silicone casting combined with 3D printing technology. Through insert molding techniques, rigid-flexible integration was realized. During locomotion, this frame dynamically anchors to the supporting surface and coordinates with flexible vacuum suckers (integrated at both ends of telescopic air bladders) to establish a spatially stable polygonal support structure. It provides essential supporting force via single-sidewall adhesion without requiring comprehensive or multi-point contact with the pipe wall, which makes SMART-PIPEBOT particularly suitable for large-diameter pipe environments. Crucially, during movement, the tail frame continuously supplies anti-overturning torque and auxiliary pivot points, significantly enhancing SMART-PIPEBOT's vertical climbing stability.

Experiments optimized the vacuum sucker mounting angle, confirming 30° as optimal, and validated climbing performance in horizontal (16.93 mm/s) and vertical (12.63 mm/s) pipes (the mean values for the Ø170 mm, Ø200 mm, and Ø230 mm pipe environments). To simulate real inspection environments, the robot maintained continuous motion under wet-wall conditions (residual clean water), achieving a mean horizontal speed of 4 mm/s (23.6% of dry conditions) and a vertical speed of 1.98 mm/s (15.7%). Gradient payload tests confirmed that when inspection equipment was fixed to the rigid vacuum sucker bracket at SMART-PIPEBOT's rear, the effective payload significantly increased to 2 times that of the front-mounted solution horizontally (100 g vs. 50 g) and 1.5 times vertically (30 g vs. 20 g), providing an optimized sensor layout solution for practical engineering. Compared to existing soft pipe robots relying on multi-point/comprehensive pipe-wall contact (e.g., [10, 11, 12, 15, 16, 18, 19, 20, 21, 22, 24, 28] requiring ≥3-point or annular support), the bionic tail support mechanism enables single-sidewall adhesion, with the following advantages:

(1) Diameter-independent compact design: Core structure maintains minimal dimensions without scaling with pipe diameter, contrasting traditional approaches requiring diameter-proportional sizing [6, 15].

(2) Energy-efficient actuation: Simplified drive system with single pneumatic unit outperforms multi-chamber drives [10, 12, 16, 18, 19, 22] and multi-module coordination [11, 15, 20, 21, 24].

(3) Enhanced large-diameter navigation: Unique load distribution mechanism overcomes bulkiness limitations of multi-point support systems [10, 15, 16, 19, 20].

(4) Pipe-friendly interaction: Flexible adhesion significantly reduces mechanical damage risks compared to rigid wheels [6, 7, 10] or mechanical anchors [11, 19, 20, 31].

2. SMART-PIPEBOT Design

SMART-PIPEBOT comprises an inflatable bladder, vacuum sucker brackets, silicone vacuum suckers, a constraining layer, and a tail support frame, as illustrated in Fig. 1(a). The inflatable bladder is fabricated using addition-cure silicone rubber molded by casting, exhibiting excellent elasticity. The end faces are equipped with air inlets, enabling inflation-driven expansion of the inflatable bladder to serve as the robot's driving source. Two poly-lactic acid (PLA)-material vacuum sucker brackets are rigidly integrated with the inflatable bladder end faces via insert molding techniques. Each bracket mounts two bellows-type silicone vacuum suckers, enabling locomotion and climbing through coordinated actuation of inflatable bladder inflation and vacuum sucker adsorption. Inspired by the woodpecker's tail-assisted support principle (see Fig. 1(b)), a tail support frame is designed and manufactured by 3D printing with PLA material. This frame is bolted to the rear vacuum sucker bracket, with its thickness adjustable according to payload requirements.

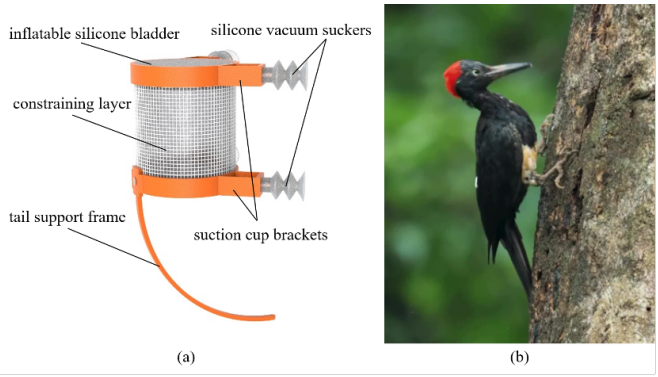

Figure 1: Schematic diagram of SMART-PIPEBOT with bio-inspired woodpecker tail support mechanism: (a) Structural composition of the robot; (b) Woodpecker tail feather-assisted support.

To adapt to large-diameter pipe environments, SMART-PIPEBOT employs a driving structure design based on an inflatable bladder. The inflatable bladder is fabricated from addition-cure silicone rubber with a selected shore hardness of 50 HA, offering excellent toughness and tensile resistance. The inflatable bladder is designed as a hollow cylindrical configuration, with its wall thickness featuring axial gradient variation: thicker near the vacuum sucker end and relatively thinner at the distal end. This asymmetric structural design enables controllable bending deformation during inflation, effectively facilitating contact and adsorption between the vacuum suckers and the pipe wall. The driving gas is controlled through air inlets at the center of the end faces for inflation and deflation.

In the inflated state, the inflatable bladder's radial wall thickness is relatively thin, leading to significant radial expansion, while axial elongation is comparatively limited. To optimize the deformation mode and enhance axial displacement for increased stepping distance, a glass fiber mesh (diameter: 0.5 mm, aperture: 2.6 mm) constraining layer is precisely wrapped around the inflatable bladder's outer wall. This constraining material exhibits excellent tensile strength (500 - 650 N/100 cm^2), effectively suppressing radial expansion, while its minimal linear density (50 g/m) ensures negligible additional weight. This design directs the pneumatic energy primarily toward axial extension, significantly improving driving efficiency.

The connection between both ends of the inflatable bladder and the vacuum suckers is realized via specially designed 3D-printed PLA vacuum sucker brackets. As a critical adapter between the rigid vacuum sucker base and the flexible inflatable bladder, the reliable sealed connection between the bracket and the inflatable bladder is achieved through insert molding techniques: The bracket is pre-positioned in the mold before the silicone inflatable bladder solidifies, allowing liquid silicone to fully infiltrate and envelop the bracket, forming a robust integrated structure after curing.

The adsorption units employ bellows-type silicone vacuum suckers, whose corrugated structure provides excellent adaptability and adsorption performance on the curved surfaces of the inner pipe wall. They are arranged in a grouped configuration to enhance adsorption stability.

To address reduced adsorption reliability due to gravitational effects during vertical climbing, especially under payload conditions, a 3D-printed PLA (elastic modulus: 3500 MPa) tail support frame was designed. This frame, together with the front and rear adsorption units, forms a stable mechanical support structure with at least three points, effectively distributing part of the load's gravity to the pipe wall, as illustrated in Fig. 2.

During the robot's vertical climbing process, the front and rear vacuum sucker groups coordinate with the driving inflatable bladder through alternating adsorption and detachment from the pipe wall to achieve a stepping motion. However, when the rear vacuum sucker group remains adsorbed while the front group detaches, the robot's total gravity G generates a significant overturning moment M_1 at the rear adsorption point. The friction force acting on the rear vacuum suckers is denoted as f (the pipe inner wall is assumed to be sufficiently smooth, and the friction between the tail support frame and the pipe wall is therefore neglected). Given that the vacuum suckers are made of flexible silicone material with limited rigidity, they cannot independently resist this overturning moment, potentially

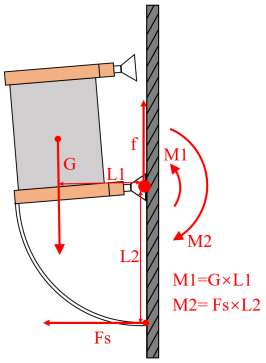

Figure 2: Principle and force analysis of the tail support frame.

causing the robot to experience backward tilting or even detach from the pipe wall.

The tail support frame is introduced precisely to resolve this stability issue. The PLA tail-support frame (semi-circular arc profile) is rigidly fixed to the upper end of the rear vacuum sucker bracket (rigid structure). Its opposite end features a tapered tip. When the overturning moment M_1 induces backward tilting, the tapered tip contacts the inner pipe wall. Upon contact, the frame applies a supporting force perpendicular to the contact surface. According to Newton's third law, the pipe wall exerts an equal and opposite reaction force F_s on the frame. A lever arm exists between the frame-wall contact point and the rear suction-cup contact, generating a counter-overturning moment (frame tip contact) and the rear vacuum sucker's adsorption point, producing a counter-overturning moment M_2 opposing M_1. When $M_2 = M_1$ is achieved, static equilibrium is established, effectively suppressing backward tilting. Thus, by providing an auxiliary pivot and generating M_2, the tail frame significantly enhances stability during critical stepping moments (rear-only adsorption), preventing detachment caused by insufficient vacuum sucker rigidity.

The tapered tip optimization converts pipe-wall contact from surface to line contact, ensuring adequate support strength while significantly reducing sliding friction resistance. The tail frame's strength can be customized via 3D printing according to specific payload requirements. Bolt-fastened to the vacuum sucker bracket, it allows convenient disassembly and replacement.

To determine the optimal tail support frame structure, three different support configurations were designed, with arc curvature radii set to be smaller than (see Fig. 3(a)), equal to (see Fig. 3(b)), and larger than (see Fig. 3(c)) the robot height (107 mm), respectively, to achieve conformal contact with the pipe wall. In the ANSYS simulation environment, a hinge structure was used to simulate the actual force state of the robot when relying on the rear vacuum sucker for adhesion. The elastic modulus of PLA used in the simulation was set to 3500 MPa. Identical boundary conditions and load parameters were applied to the three tail support frames to evaluate their support force and deformation response. The results from Fig. 3 show that: when the tail support frame has shape (a), it provides approximately 0.38 N of support force with relatively low deformation; shape (b) provides approximately 0.45 N of support force with moderate deformation; and shape (c) provides approximately 0.33 N of support force but exhibits significant deformation. Comprehensive analysis indicates that the tail support frame constructed with an arc radius equal to the robot height (i.e., structure (b)) offers a more ideal support force while ensuring relatively small deformation, thus demonstrating superior mechanical performance and structural adaptability.

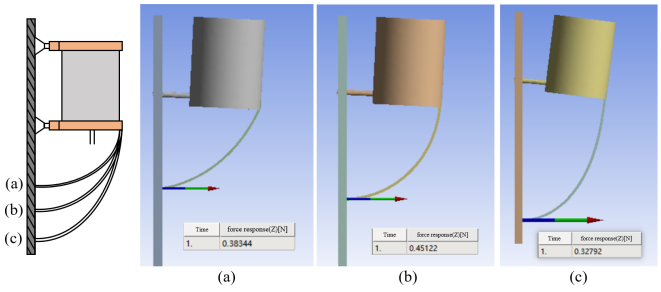

Figure 3: Simulation results of tail support frames with different shapes: (a) radius smaller than 107 mm; (b) radius equal to 107 mm; (c) radius larger than 107 mm.

3. Operating Principle and Fabrication

3.1. Driving Principle of the Robot

The driving principle of SMART-PIPEBOT is based on the periodic deformation of an inflatable bladder coordinated with alternating vacuum sucker actuation. The motion sequence is illustrated in Fig. 4. In the initial state (see Fig. 4(a)), the inflatable bladder is exhausted and contracted, while the rear vacuum sucker remains adsorbed onto the pipe wall. Upon initiation of the driving cycle, the inflatable bladder is inflated to achieve axial extension (see Fig. 4(b)). This deformation drives the front vacuum sucker assembly forward. Once the inflatable bladder deformation reaches its maximum (see Fig. 4(c)), the front vacuum sucker is subsequently activated and adsorbed onto the pipe wall, while the rear vacuum sucker simultaneously releases its adsorption. In the final stage (see Fig. 4(d)), the inflatable bladder is exhausted and contracts to its initial form due to the elastic restoring force of the silicone material. This process pulls the released rear vacuum sucker assembly forward, thereby completing one full stepping motion cycle. By repeating this cyclic sequence, the robot achieves continuous motion along the pipe axis.

3.2. Fabrication and Assembly

During the analysis of flexible inflatable bladder materials, the material for the telescopic part of the soft robot requires good sealing properties and the ability to withstand sufficient internal pressure to meet basic operational requirements. We selected OTHER-001 addition-cure silicone rubber with a Shore hardness of 50 HA as the primary material. This silicone was selected for its low density, ease

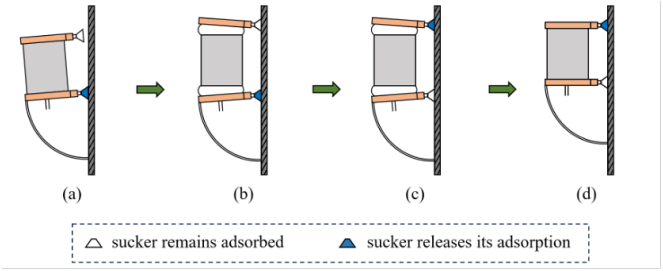

Figure 4: Schematic of the robot's driving principle: (a) Rear vacuum sucker remains adsorbed, and tail support frame provides support; (b) Inflatable bladder inflates and drives front assembly forward in axial extension; (c) Front vacuum sucker adsorbs while rear vacuum sucker releases adsorption; (d) Inflatable bladder exhausts and pulls rear assembly forward.

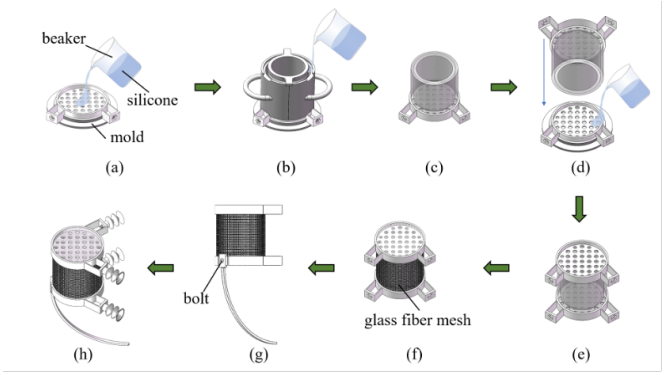

Figure 5: Fabrication process of SMART-PIPEBOT: (a) Pour the mixed silicone into the mold; (b) Pour the mixed silicone into the mold to bond with the cured silicone rubber component; (c) Remove the mold to obtain a semi-finished part; (d) Pour the mixed silicone into the mold to bond with the semi-finished part; (e) Remove the mold to obtain the primarily formed robot structure; (f) Wrap the glass fiber mesh layer around the exterior of the robot; (g) Fix the tail support frame to the robot with bolts; (h) Robot fabrication is completed.

of molding, and adequate sealing performance under the target pressure range. It can be molded into application-specific geometries while maintaining high compliance.

Furthermore, to connect the inflatable bladder to the vacuum suckers, this paper employed PLA material fabricated via 3D printing. This material exhibits excellent tensile strength and ductility, yielding brackets with superior mechanical and physical properties that effectively support the robot's needs in various working environments. By selecting appropriate materials, SMART-PIPEBOT not only possesses the necessary functionality but also ensures reliability and durability in practical applications.

SMART-PIPEBOT is manufactured by casting silicone solution into molds. The fabrication process primarily involves two key steps: first, manufacturing molds using 3D printing technology; second, casting the silicone rubber solution into the molds to form the soft robot. The main preparation steps are illustrated in Fig. 5. SMART-PIPEBOT is fabricated using a multi-step molding process centered on addition-cure silicone rubber with a Shore hardness of 50 HA. The process begins with creating a rigid-flexible integrated vacuum sucker bracket by pouring the mixed and degassed silicone into a 3D-printed honeycomb mold and heat-curing it. Subsequently, this cured bracket is assembled with outer and core molds for a second silicone pouring and thermal curing to form the main inflatable bladder wall, achieving a seamless, integrated structure. After demolding the primary silicone body, a glass fiber mesh is wrapped around the inflatable bladder and secured with nylon thread to constrain radial expansion and enhance axial driving efficiency. Finally, the assembly is completed by bolting the 3D-printed PLA tail support frame onto the rear vacuum sucker bracket and installing the FG20 silicone vacuum suckers and necessary air tubes.

4. Experimental Methods and Results

4.1. Effect of Vacuum-Sucker Inclination on Adhesion Force

This experiment quantifies the relationship between the included angle of the vacuum suckers within a vacuum sucker group and the maximum tensile load capacity of SMART-PIPEBOT, thereby determining the optimal vacuum sucker angle for maximizing the adsorption force. Based on the schematic in Fig. 6 illustrating vacuum sucker angular positioning principles, the adsorption effect and success rate are optimal when the vacuum sucker axis is perpendicular to the tangent direction of the pipe inner wall [36]. To systematically explore how the adsorption force varies with vacuum sucker orientation, let α be the included angle between the vacuum sucker axis and the pipe centerline, as depicted in Fig. 6. To better investigate the selection range of the included angle of the vacuum suckers, a computational discussion on the relationship between the included angle of the vacuum suckers and their mounting position is conducted as follows.

Circle O represents the robot, and circle O' represents the pipeline. The robot is placed inside the pipeline. $O'A$ is the radius of the pipeline, and since the adsorption effect is optimal when the axis of the vacuum sucker is perpendicular to the inner wall of the pipeline, $O'A$ also determines the direction of the vacuum sucker, with the vacuum sucker angle denoted as α. The length of AB is l, which represents the height of the vacuum sucker and depends on the model of the vacuum sucker. To investigate the relationship between the vacuum sucker angle α and the adsorption force, it is necessary to derive the relationship between α and the position of the vacuum sucker. Here, point B is considered as the fixed position of the vacuum sucker, and point O is taken as the coordinate origin to establish a parametric equation with respect to α.

For the horizontal coordinate of point B, a perpendicular line is drawn from point B to the extension line of $O'O$, intersecting at point C. The following can be obtained:

$$x(\alpha) = (O^{'}A - AB)\sin\alpha \tag{1}$$

Regarding the vertical coordinate of point B, a perpendicular line is drawn from point A to the extension line of $O'O$, intersecting at point D, and then connecting AO. The following can be obtained: $AD = O^{'}A\sin\alpha$, where OA represents the distance from the vacuum sucker to the center of the robot's airbag. This distance is determined by the diameter of the airbag and the length of the vacuum sucker, making OA a fixed value. In ΔOAD, the following can be derived: $OD = \sqrt{OA^2 - AD^2}$.

Draw a perpendicular line from point B to line AD, intersecting at point E. It can be concluded that $\alpha = \angle ABE$, and the following can be obtained: $CD = BE = AB\cos\alpha$. Therefore, the following can be obtained:

$$y(\alpha) = AB\cos\alpha - \sqrt{OA^2 - AD^2}. \tag{2}$$

Finally, taking O' as the coordinate origin, the parametric equations for the coordinates of point B with respect to α are:

$$\begin{cases} x(\alpha) = (O^{'}A - AB)\sin\alpha \\ y(\alpha) = AB\cos\alpha - \sqrt{OA^2 - (O^{'}A\sin\alpha)^2} \end{cases} \tag{3}$$

Taking the 200 mm pipe diameter selected in the experiment as an example, the height of the selected vacuum sucker is 30 mm, and the distance from the vacuum sucker to the center of the robot's inflatable bladder is measured to be 80 mm. When α is 10°, the calculated value is $x(\alpha) = 12.16$ mm. If $\alpha < 10°$, the value of $x(\alpha)$ decreases. Due to the thickness of the vacuum sucker bracket itself, interference between the two vacuum sucker brackets may occur. When α is 50°, the calculated value is $y(\alpha) = -3.08$ mm. If $\alpha > 50°$, the value of $y(\alpha)$ decreases, causing the vacuum suckers to move closer to the sides of the robot. This brings the main body of the robot (particularly the inflatable bladder) closer to the opposite pipe wall, increasing the risk of unintended contact or interference.

Within a reasonable range, five experimental conditions with different angles (10°, 20°, 30°, 40°, 50°) are designed. To ensure consistent test conditions and to rigorously maintain the critical posture where the vacuum sucker axis remains perpendicular to the pipe wall tangent across all angles, specialized PLA vacuum sucker brackets with stepped sliding rails (corresponding to the five preset angles) and matching sliders (see Fig. 7) are fabricated via 3D printing. The sliders are securely fastened to the rails using bolts, enabling precise and reliable angular positioning and fixation during testing.

To measure the external load capacity under different included angles, a simulated tensile-load test platform incorporating a force sensor is designed, as shown in Fig. 8. The pipe and a linear guide rail are fixed to a horizontal table.

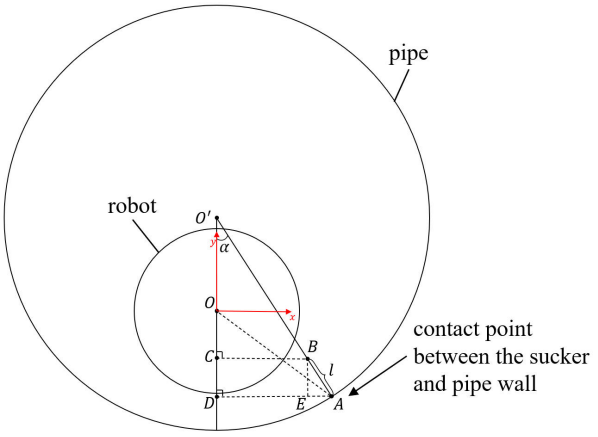

Figure 6: Calculation of the relationship between the included angle of the vacuum suckers and their mounting position.

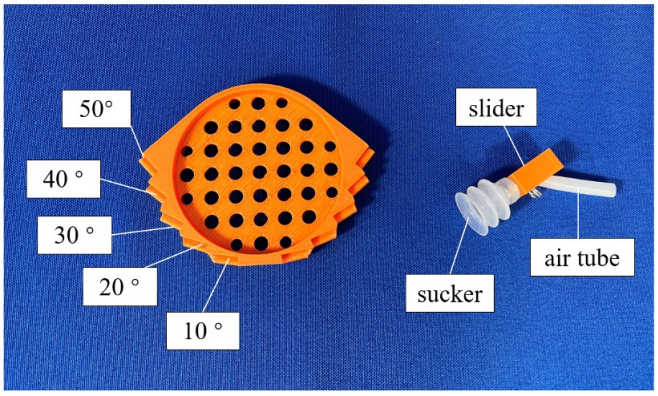

Figure 7: Sucker-mounted slider mated to the variable-angle sucker bracket.

A digital force sensor is bolted to the slider on the linear guide rail. The robot is placed inside the pipe, connected via an axial PLA bracket to a nylon line attached to the force sensor's hook. As analyzed previously, changes in the vacuum sucker angle induce corresponding variations in the robot's radial position within the pipe (the distance from the inflatable bladder axis to the pipe wall): an increased angle reduces the robot's overall height. To ensure the robot's axis remains collinear with the tensile force direction (strictly horizontal) across all angle conditions, eliminating interference from non-axial force components, an adjustable-height shim set is installed at the base of the tensile test setup. Shim thicknesses, calculated specifically for each vacuum sucker angle, effectively compensate for height variations caused by angle changes, achieving consistent tensile loading direction control across test groups.

To minimize experimental error and avoid randomness, five adsorption force tests were conducted for each preset angle group (10°, 20°, 30°, 40°, 50°). Fig. 9 shows the distribution characteristics of the adsorption force from the five tests at different angles.

As shown in Fig. 9, the adsorption force within the pipe peaks at a 30° vacuum sucker angle under identical air

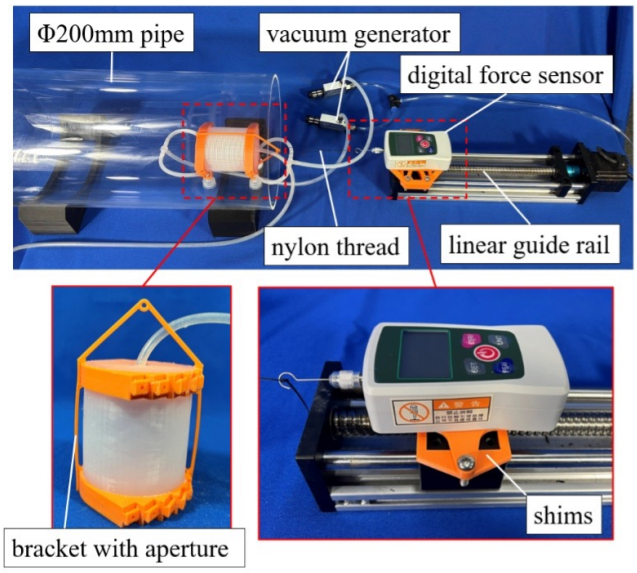

Figure 8: Adsorption force test platform.

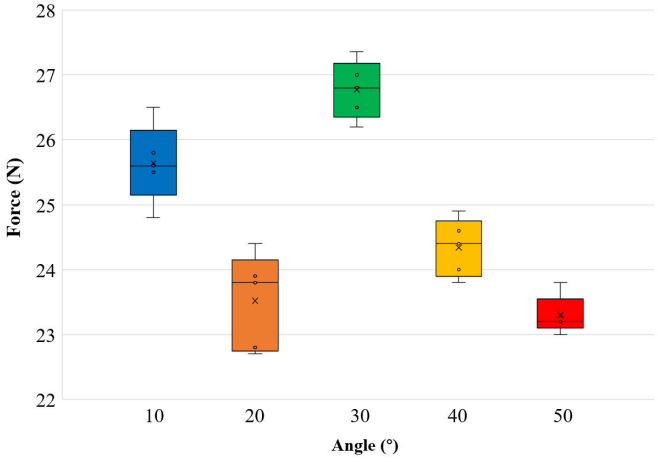

Figure 9: Adsorption force results from multiple measurements at different vacuum sucker angles.

pressure, averaging 26.778 N. Angles of 10° and 40° yield lower values, while 20° and 50° perform significantly worse, reaching only 22.592 N. At smaller included angles (e.g., 10° and 20°), the robot's overall height increases, raising its center of gravity. The horizontally applied tensile force acting on the robot's axis generates a larger overturning torque due to the increased lever arm between the force application point and the vacuum sucker adsorption points. The resulting moment promotes edge peeling, which degrades sealing and reduces vacuum level, decreasing adhesion force. At larger included angles (e.g., 40° and 50°), the robot's reduced height increases the likelihood of unintended rigid contact or interference between the robot's structural components (inflatable bladder or brackets) and the pipe inner wall. This contact disrupts the ideal conformal contact between the vacuum suckers and the pipe wall, preventing the formation of an effective, complete sealing zone. This limitation restricts the theoretical maximum adsorption force and significantly degrades the system's effective load capacity.

Therefore, an optimal included angle (30° in this experiment) exists that balances the avoidance of excessive overturning moments and structural interference, thereby maximizing adsorption force. The experiment concludes that a 30° vacuum sucker bracket angle enables the robot to achieve its maximum tensile resistance during adsorption.

4.2. Locomotion in Dry Pipes: Horizontal and Vertical Climbing

We evaluate the locomotion capabilities of SMART-PIPEBOT in mock-up pipeline environments, obtaining key motion performance parameters through empirical measurements to validate the feasibility and pipeline adaptability of the soft robot.

Testing is conducted under two configurations: horizontally and vertically oriented acrylic pipes. Considering that the axis of the vacuum sucker remains perpendicular to the tangent direction of the pipe inner wall, evaluation scenarios are designed for three different pipe diameters, corresponding to acrylic pipes with inner diameters of 170 mm, 200 mm, and 230 mm. To quantify the pipe traversal capability of SMART-PIPEBOT, a test platform is constructed as shown in Fig. 10, comprising a pipe support frame, a transparent acrylic pipe, an STM32 microcontroller-based control system, relays, solenoid valves, vacuum generators, precision throttle valves, an air supply source, a power supply, and a host computer. Transparent acrylic pipes are employed to facilitate experimental observation.

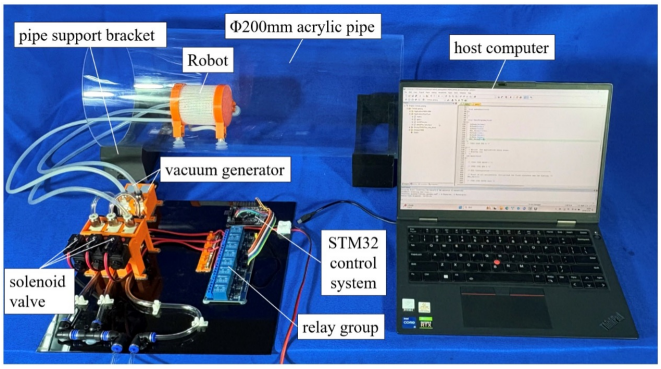

Figure 10: Experimental apparatus and testing platform.

SMART-PIPEBOT utilizes compressed air as its driving power source, with motion performance closely dependent on gas flow rate and pressure parameters. A pneumatic circuit (see Fig. 11) is designed to meet actuation requirements, incorporating precision pressure regulators, throttle valves, and 3-port 2-position solenoid valves to establish a stable and controllable pneumatic system.

During testing at an operating pressure of 0.05 MPa—a value determined through experimental optimization to balance between ineffective actuation at lower pressures and

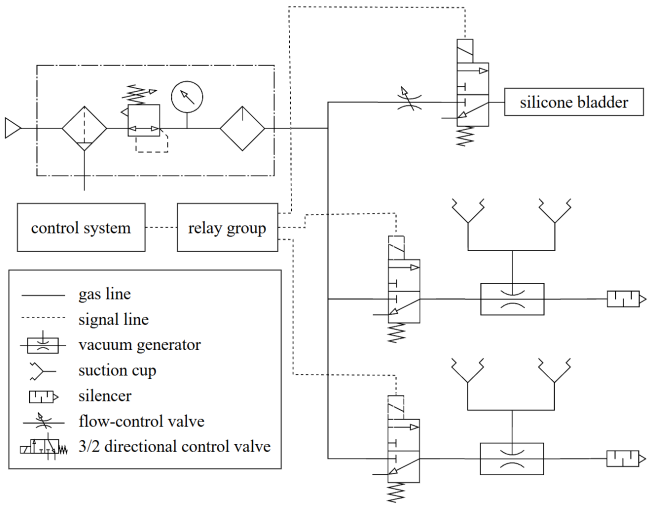

Figure 11: Pneumatic circuit of the experimental testing platform.

Table 1
Robot motion data in different pipe diameters.

Pipe Size	Horizontal Speed	Vertical Speed
170 mm	16 mm/s	12.2 mm/s
200 mm	18 mm/s	12.7 mm/s
230 mm	16.8 mm/s	13 mm/s

control challenges at higher ones—the robot's climbing capability in both orientations is demonstrated in Figs. 12 and 13. As detailed in Tab. 1, SMART-PIPEBOT achieves a mean horizontal climbing speed of 16.93 mm/s inside the pipe with no observed slipping phenomena. Despite significant differences in frictional forces between configurations, the vertical climbing speed remains notably high, averaging 12.63 mm/s without substantial reduction.

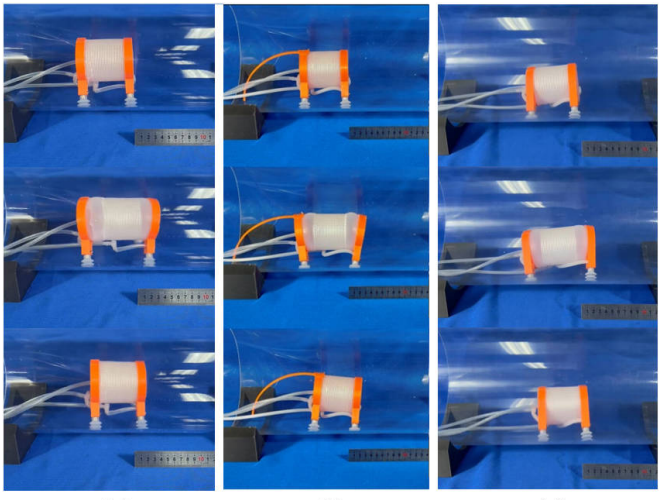

Figure 12: Locomotion performance of SMART-PIPEBOT during one cycle in horizontal acrylic pipe: (a) Ø170 mm pipe; (b) Ø200 mm pipe; (c) Ø230 mm pipe.

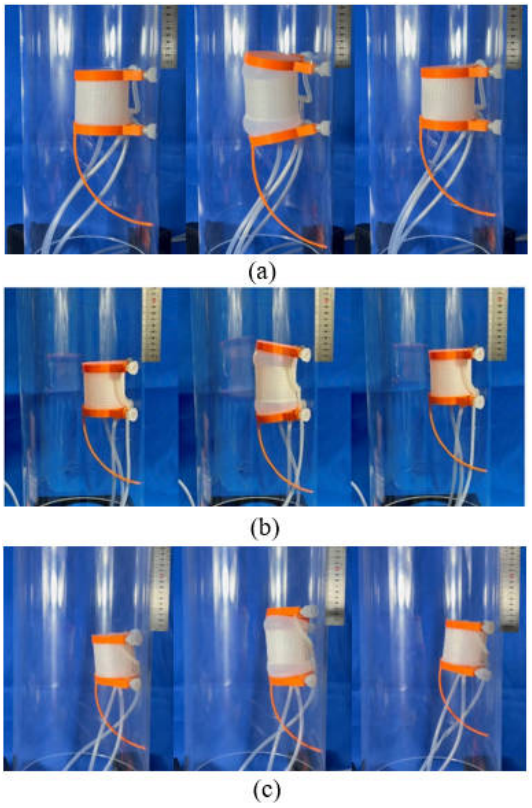

Figure 13: Climbing performance of SMART-PIPEBOT during one cycle in vertical acrylic pipe: (a) Ø170 mm pipe; (b) Ø200 mm pipe; (c) Ø230 mm pipe.

Table 2
Robot's locomotion speed in clean-water pipes of various diameters.

Pipe Size	Horizontal Speed	Vertical Speed
170 mm	4 mm/s	1.89 mm/s
200 mm	4.1 mm/s	2 mm/s
230 mm	3.8 mm/s	2.1 mm/s

4.3. Locomotion in Wet Pipes with Residual Water Films

In accordance with pipeline inspection safety regulations, media drainage is required before defect detection (cracks, corrosion) to eliminate potential hazards. To simulate practical post-drainage conditions with residual liquid films on pipe walls, we establish a clean-water residual environment to systematically assess the robot's motion stability and traversability.

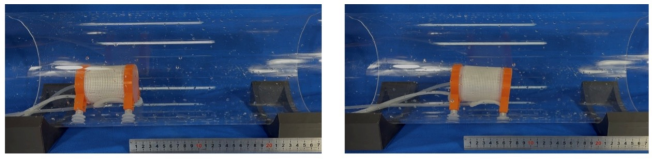

Figure 14: Robot's horizontal motion in a clean-water pipeline.

First, a horizontal pipeline condition with residual clean water was established. Clean water was uniformly sprayed onto the inner wall of a horizontally oriented acrylic pipe, after which the robot was placed inside. Its motion was captured using high-speed video, as shown in Fig. 14. The mean speeds over multiple cycles were calculated for three pipe diameters, namely 170 mm, 200 mm, and 230 mm, as reported in Tab. 2. The results indicate a mean displacement of 6 mm per cycle with a cycle duration of 1.5 s, giving a mean locomotion speed of 4 mm/s under these conditions.

Subsequently, a vertical pipeline condition with residual clean water was established. The pipe wall was uniformly wetted, the pipe was oriented vertically, and the robot was then introduced. The climbing sequence is shown in Fig. 15. SMART-PIPEBOT maintained stable upward locomotion. As reported in Tab. 2, the mean displacement per cycle was 3.37 mm with a cycle period of 1.7 s, corresponding to a mean climbing speed of 1.98 mm/s. Relative to horizontal operation, the vertical orientation yielded a smaller cycle displacement because the robot must work against gravity, while continuous climbing performance was still achieved.

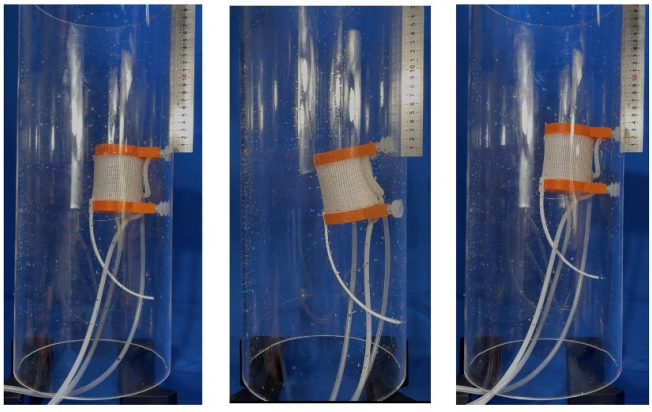

Figure 15: Robot's vertical motion in clean-water pipelines.

The experiments indicate that residual liquid films markedly degraded locomotion performance. In wet pipes, SMART-PIPEB mean speed decreased by 76.4% in the horizontal configuration, from 16.93 to 4 mm/s, and by 84.3% in the vertical configuration, from 12.63 to 1.98 mm/s.

In horizontal pipes, the liquid film can fill microscopic gaps between the vacuum sucker and the pipe wall, creating a transient sealing layer that slightly increases the effective vacuum adsorption relative to dry conditions. However, viscous resistance from the water impedes vacuum sucker release. During inflatable bladder contraction, the robot must overcome the viscous film to detach and reset, which substantially prolongs the reset phase compared with dry operation. The reduced displacement per cycle, therefore, arises mainly from disrupted gait timing due to detachment hysteresis, indicating that the dominant limitation in horizontal wet pipes is not insufficient adsorption, but the increased energy and time required for detachment.

In vertical pipes, the liquid film introduces additional adverse effects. Wet surfaces reduce the effective static friction between the vacuum suckers and the pipe wall, thereby weakening anti-slip capability. Although vacuum adsorption may be enhanced by the sealing effect, lubrication reduces tangential traction, so the available adhesion becomes insufficient to balance the downward components of self-weight and any payload. Intermittent slippage was observed during climbing, which substantially limited the displacement per cycle, and accumulated slip led to complete detachment in some trials. Despite these challenges, SMART-PIPEBOT retained continuous locomotion under wet wall conditions, supporting its practicality for inspection tasks after pipeline drainage.

4.4. Payload Capacity and Mounting-Location Effects

In practical pipeline inspection tasks, robots typically need to carry onboard sensors and detection modules for defect identification. To evaluate SMART-PIPEBOT's locomotion performance and operational feasibility under payload conditions, external loads were applied at different locations on the robot body, and the resulting motion behavior was experimentally assessed.

Given the rigid structure of the front/rear vacuum sucker bracket contrasted with the flexible inflatable bladder (which undergoes significant deformation during actuation), optimal payload mounting positions were identified at the rigid vacuum sucker bracket. A custom load-bearing bracket was fabricated via 3D printing and alternately mounted onto the front and rear vacuum sucker brackets. Precision weights were secured using elastic straps, with specific configurations shown in Fig. 16.

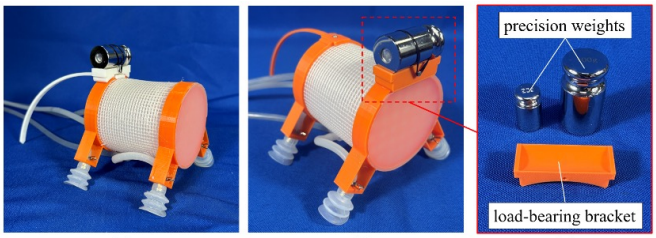

Figure 16: Load-bearing bracket and weights mounted on front/rear vacuum sucker bracket: (a) Load-bearing bracket fixed on rear vacuum sucker bracket; (b) Load-bearing bracket fixed on front vacuum sucker bracket; (c) Load-bearing bracket with precision weights.

Five graded payload conditions, namely 10 g, 20 g, 50 g, 100 g, and 200 g, were tested to systematically assess load-carrying capability. With the payload mounted at the front, SMART-PIPEBOT exhibited stable locomotion in horizontal pipes (see Fig. 17(a)) at normal speed up to 100 g, but failed at 200 g due to excessive deformation of the front section. In vertical pipes (see Fig. 18(a)), the maximum effective payload was 20 g. Increasing the payload to 50 g shifted the center of gravity and induced a pitch-up motion

at the front end, which reduced the effective contact area of the vacuum sucker and led to detachment.

Using the same procedure, the load-bearing bracket was then mounted at the rear. In horizontal pipes (see Fig. 17(b)), stable locomotion at normal speed was maintained with a 100 g payload, whereas failure occurred at 130 g. In vertical pipes (see Fig. 18(b)), the maximum effective payload increased to 30 g. When the payload was increased to 50 g, the tail support frame was unable to generate sufficient counter overturning moment, and the robot failed to climb.

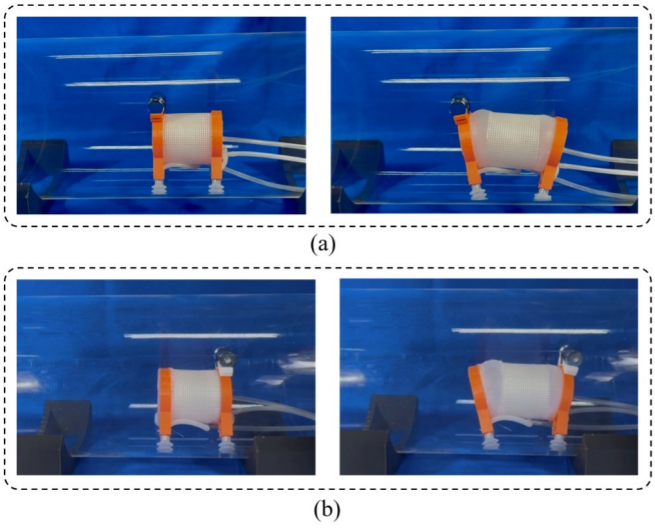

Figure 17: Robot's payload motion test in horizontal pipes: (a) Load-bearing bracket fixed on front vacuum sucker bracket; (b) Load-bearing bracket fixed on rear vacuum sucker bracket.

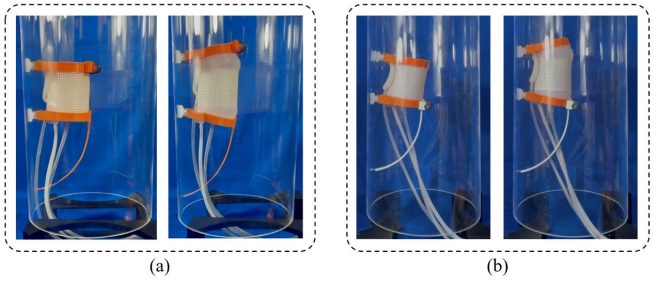

Figure 18: Robot's payload motion test in vertical pipes: (a) Load-bearing bracket fixed on front vacuum sucker bracket; (b) Load-bearing bracket fixed on rear vacuum sucker bracket.

The experiments show that SMART-PIPEBOT can sustain substantially larger payloads when the load is mounted at the rear rather than at the front. This difference is primarily attributable to the load-induced moment distribution. A front-mounted payload concentrates the added mass on the upper section of the robot at point a in Fig. 19, which produces a longer moment arm than an equivalent load applied at the rear at point b in Fig. 19. The resulting increase in bending moment acts on the tail support frame and can exceed its effective stiffness, leading to progressive deformation and reduced stability. By contrast, when the payload is rear-mounted, the induced moments are borne more effectively by the drive assembly, which has higher structural rigidity. This reduces the destabilizing effect of the payload and, consequently, lowers the additional power required to maintain locomotion.

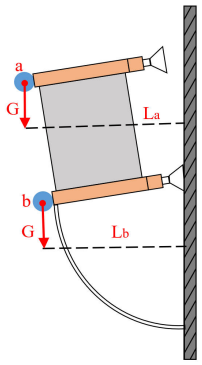

Figure 19: Force Analysis Under Different Load Positions

5. Discussion

5.1. Design Advantages and Practical Implications

Relative to prior soft in-pipe robots that rely on multi-point or comprehensive pipe-wall contact support (e.g., annular expansion anchoring [10, 12, 16, 18, 19, 22, 24, 26, 28, 30, 31], multi-tentacle support [15, 16, 20, 21, 23], or multi-chamber coordination [10, 11, 16, 18, 19, 22, 28]), SMART-PIPEBOT offers:

(1) Structural lightweighting and diameter decoupling: The lever effect of the tail support frame effectively distributes loads, enabling stable operation via single-sidewall adhesion in large-diameter pipes (170 mm, 200 mm, and 230 mm) (mean horizontal speed: 16.93 mm/s; mean vertical speed: 12.63 mm/s). The robot's compact core structure (length $\approx$ 20 cm, width $\approx$ 13 cm, weight $\approx$ 80 g) requires no significant scaling with increasing pipe diameter, overcoming the bulkiness, reduced flexibility, and surging energy consumption of traditional multi-point support solutions in large-diameter environments [10, 15, 16, 19, 20, 21, 24, 26, 33].

(2) Drive simplification and low energy consumption: Only a single inflatable bladder unit and two pairs of vacuum suckers are required (driving pressure: 0.05 MPa). The point/line contact friction resistance of the tail support frame remains low. Compared to complex systems requiring multi-chamber or multi-module coordinated drives [10, 11, 12, 15, 16, 18, 19, 20, 21, 22, 24, 26, 28, 30], this design significantly reduces system complexity, control difficulty, and overall energy consumption.

(3) Superior large-diameter adaptability: The anti-overturning torque and auxiliary pivot points provided by the tail support frame are critical for stable climbing (especially vertical climbing) in large-diameter pipes, offering an efficient solution for inspecting large pipelines (e.g., urban drainage mains, oil/gas transmission pipes).

(4) Low pipe-wall damage risk: The tapered tip optimization (converting contact to line contact) combined with flexible vacuum sucker contact significantly reduces mechanical damage risks to pipe walls, outperforming rigid wheel-based [6, 7, 10] or mechanical anchoring solutions [11, 16, 19, 20, 21, 30, 31].

5.2. Limitations and Future Work

Although SMART-PIPEBOT demonstrates strong performance in large-diameter rigid pipes, several potential limitations remain and could be addressed through the following future improvements:

(1) Dependency on Pipe Material: The current vacuum suckers exhibit insufficient sealing on porous, rough, or non-rigid pipes (e.g., concrete/soft plastic pipes). Future iterations could adopt foam suckers or other solutions better suited to irregular surfaces to enhance adaptability.

(2) Performance Degradation in Wet Environments: Clean-water residual tests indicate that liquid films significantly reduce locomotion performance. Optimizing sucker materials (e.g., hydrophobic coatings) or control strategies may mitigate this issue.

(3) Locomotion Speed and Payload Capacity: Future work could involve using lighter materials to reduce robot weight, as well as exploring onboard energy storage or more flexible tubing solutions to improve speed and effective payload.

(4) Adaptability to Complex Pipelines: The current robot has limited degrees of freedom, making it difficult to traverse pipe bends. Redesigning the driving structure into a multi-segment configuration with independently controllable pneumatic chambers presents a promising solution for achieving bending and steering capabilities.

(5) Optimization of Friction Utilization in the Tail Support Mechanism: On rough surfaces, the friction effect of the tail support frame is dual-sided. Future efforts will focus on optimizing its contact geometry and materials to maximize beneficial friction during the support phase while minimizing resistive friction during the return stroke.

6. Conclusion

This paper presents SMART-PIPEBOT, a novel bio-inspired soft pipe-climbing robot that incorporates a woodpecker-tail-like elastic support mechanism to achieve stable single-sidewall adhesion in large-diameter pipes. SMART-PIPEBOT has been fabricated using silicone casting and 3D printing to realize rigid and compliant components within an integrated structure. Experimental optimization identified a 30° vacuum-sucker angle, which yields a maximum mean adsorption force of 26.778 N. With a driving pressure of 0.05 MPa, SMART-PIPEBOT operates reliably and achieves mean climbing speeds of 16.93 mm/s in horizontal pipes and 12.63 mm/s in vertical pipes. By combining a bionic support strategy with an optimized suction mechanism and a streamlined fabrication process, the proposed design offers a compact, energy efficient, and pipe-friendly solution that addresses the limitations of conventional robots that rely on multi-point contact for large diameter pipeline inspection.

SMART-PIPEBOT has demonstrated continuous motion even under wet-wall conditions, though speeds decreased to 23.6% (horizontal) and 15.7% (vertical) of dry-condition performance, confirming its feasibility in post-drainage inspection environments. Payload tests reveal that rear-mounting inspection equipment significantly enhanced load capacity, supporting up to 100 g horizontally and 30 g vertically—double and 1.5 times the front-mounted capacity, respectively. These results validate SMART-PIPEBOT's ability to maintain climbing stability while carrying practical loads.

Acknowledgements

This work was supported in part by The Royal Society under Grant IES/R2/232291, the UK-RAS Network+, the EPSRC (Grant number: EP/Y010523/1), and the European Commission grant Up-Skill (Horizon Europe RIA 101070666).

References

[1] B. A. Shah and A. G. A. Muthalif. A comprehensive review on corrosion management in oil and gas pipeline: methods and technologies for corrosion prevention, inspection and monitoring. *Anti-Corrosion Methods and Materials*, 2025.

[2] N. V. S. Korlapati, F. Khan, Q. Noor, et al. Review and analysis of pipeline leak detection methods. *Journal of Pipeline Science and Engineering*, 2(4):100074, 2022.

[3] B. Liu, J. He, L. Zhang, et al. Pipeline safety monitoring technology based on FBG-ROTDR joint system and its case study of urban drainage pipeline monitoring. *Optical Fiber Technology*, 73:103044, 2022.

[4] Kaned Thung-Od, Kiattisin Kanjanawanishkul, Thavida Maneewarn, Thunyaseth Sethaput, and Arsit Boonyaprapasorn. An in-pipe inspection robot with permanent magnets and omnidirectional wheels: Design and implementation. *Applied Sciences*, 12(3):1226, 2022.

[5] Mingze Gao, Min Huang, Kai Tang, Xuqiang Lang, and Jiaming Gao. Design, analysis, and control of a multilink magnetic wheeled pipeline robot. *IEEE Access*, 10:67168–67180, 2022.

[6] Hongwei Yan, Pengyang Zhao, Canjun Xiao, Dengxiao Zhang, Shaoni Jiao, Haibing Pan, and Xi Wu. Design and kinematic characteristic analysis of a spiral robot for oil and gas pipeline inspections. *Actuators*, 12(6):240, 2023.

[7] Kunlun Wu, Haifeng Sang, Yanhao Xing, and Yao Lu. Design of wireless in-pipe inspection robot for image acquisition. *Industrial Robot: the International Journal of Robotics Research and Application*, 50(1):145–161, 2023.

[8] Yongming Wang, Jinlong Wang, Qi Zhou, Sai Feng, and Xiaomin Wang. Mechanism design and mechanical analysis of pipeline inspection robot. *Industrial Robot: the International Journal of Robotics Research and Application*, 52(1):137–143, 2025.

[9] Jianlin Wang, Yixiang Wang, Lining Peng, Haixiang Zhang, Hang Gao, Chengjiang Wang, Yuan Gao, Huanliang Luo, and Yongquan Chen. Transformable inspection robot design and implementation for complex pipeline environment. *IEEE Robotics and Automation Letters*, 9(6):5815–5822, 2024.

[10] Rajendran Sugin Elankavi, D Dinakaran, Arockia Selvakumar Arockia Doss, RM Kuppan Chetty, and MM Ramya. Design and motion planning of a wheeled type pipeline inspection robot. *Journal of Robotics and Control (JRC)*, 3(4):415–430, 2022.

[11] Tao Zheng, Xiang Wang, Hui Li, Chuan Zhao, Zhihong Jiang, Qiang Huang, and Marco Ceccarelli. Design of a robot for inspecting the

multishape pipeline systems. *IEEE/ASME Transactions on Mechatronics*, 27(6):4608–4618, 2022.

[12] Kwang-Woo Jeon, Eui-Jung Jung, Jong-Ho Bae, Sung-Ho Park, Jung-Jun Kim, Goobong Chung, Hyun-Joon Chung, and Hak Yi. Development of an in-pipe inspection robot for large-diameter water pipes. *Sensors*, 24(11):3470, 2024.

[13] Heesik Jang, Tae Yu Kim, Ye Chan Lee, Yong Heon Song, and Hyouk Ryeol Choi. Autonomous navigation of in-pipe inspection robot using contact sensor modules. *IEEE/ASME Transactions on Mechatronics*, 27(6):4665–4674, 2022.

[14] Jingwei Liu, Man Li, Yahui Wang, Da Zhao, and Rui Deng. Multi-gait snake robot for inspecting inner wall of a pipeline. *Biomimetic Intelligence and Robotics*, 4(2):100156, 2024.

[15] Di Guo, Yiqiang Wang, and Zhan Kang. A hollow shell-lattice soft robot in flexible pipelines with flowing fluids. *Advanced Science*, page 2414882, 2025.

[16] Wenbiao Wang, Xin Wang, Gang Zheng, Rui Chen, Zean Yuan, Jincheng Huang, Ke Wu, and Guanjun Bao. A modular soft pipe-climbing robot with high maneuverability. *IEEE/ASME Transactions on Mechatronics*, 29(6):4734–4743, 2024.

[17] Rui Chen, Huigang Wang, Haoji Wang, Huijiang Wang, Li Bai, Xinpei Ai, Lifu Liu, Zhihao Hu, and Zean Yuan. A motion-sensing integrated soft robot with triboelectric nanogenerator for pipeline inspection. *Advanced Intelligent Systems*, 7(6):2400643, 2025.

[18] Mohd Aliff, Mohammad Imran, Sairul Izwan, Mohd Ismail, Nor Samsiah, Tetsuya Akagi, Shujiro Dohta, Weihang Tian, So Shimooka, and Ahmad Athif. Development of pipe inspection robot using soft actuators, microcontroller and labview. *International Journal of Advanced Computer Science and Applications*, 13(3), 2022.

[19] R Okuma, Y Naruse, F Ito, and T Nakamura. Peristaltic soft robot for long-distance pipe inspection with an endoskeletal structure for propulsion and traction amplification. In *2024 IEEE/RSJ International Conference on Intelligent Robots and Systems (IROS)*, pages 4053–4060. IEEE, 2024.

[20] Yunwei Zhao, Haoran Huang, Weizhe Yuan, Xiaomin Liu, and C Chase Cao. Worm-inspired, untethered, soft crawling robots for pipe inspections. *Soft Robotics*, 11(4):639–649, 2024.

[21] Xiaomin Liu, Maozheng Song, Yuhui Fang, Yunwei Zhao, and Changyong Cao. Worm-inspired soft robots enable adaptable pipeline and tunnel inspection. *Advanced Intelligent Systems*, 4(1):2100128, 2022.

[22] Yujia Li, Yu Xia, Tao Ren, Zheyi Jin, Weiye Zhuang, Xiao Huang, and Weisong Yu. A soft pipeline robot inspired by inchworm locomotion with layer-interference variable stiffness. *Smart Materials and Structures*, 34(3):035027, 2025.

[23] Zhang Yu, Huang Peiyu, You Bo, Yu Zhibin, Li Dongjie, and Dong Guoqi. Design and motion simulation of a soft robot for crawling in pipes. *Applied Bionics and Biomechanics*, 2023(1):5334604, 2023.

[24] Jing Jiang, Feng Zhang, and Lei Wang. Soft modular pipe robot inspired by earthworm for adaptive pipeline internal structure. *Smart Materials and Structures*, 33(10):105019, 2024.

[25] Deli Xia, Luying Zhang, Weihang Nong, Qingshan Duan, and Jiang Ding. 3d-printed soft bionic inchworm robot powered by magnetic force. *Biomimetics*, 10(4):202, 2025.

[26] Chao Tang, Boyuan Du, Songwen Jiang, Qi Shao, Xuguang Dong, Xin-Jun Liu, and Huichan Zhao. A pipeline inspection robot for navigating tubular environments in the sub-centimeter scale. *Science Robotics*, 7(66):eabm8597, 2022.

[27] Yangyang Du, Xiaojun Wu, Jiasheng Xue, Xingyu Chen, Chongjing Cao, and Xing Gao. A soft robot driven by a spring-rolling dielectric elastomer actuator with two bristles. *Micromachines*, 14(3):618, 2023.

[28] Qin Fang, Jingyu Zhang, Yinhui He, Nenggan Zheng, Yue Wang, Rong Xiong, Zhefeng Gong, and Haojian Lu. Drosophila larvae-inspired soft crawling robot with multimodal locomotion and versatile applications. *Research*, 7:0357, 2024.

[29] Xuanyi Zhou, Yuqiu Zhang, Zhiwei Qiu, Zhecheng Shan, Shibo Cai, and Guanjun Bao. Locomotion control of a rigid-soft coupled snake robot in multiple environments. *Biomimetic Intelligence and Robotics*, 4(2):100148, 2024.

[30] Ying Lin, Yi-Xian Xu, and Jia-Yang Juang. Single-actuator soft robot for in-pipe crawling. *Soft Robotics*, 10(1):174–186, 2023.

[31] Fumio Ito, Yuta Naruse, Kazuki Takaya, J Watanabe, and Taro Nakamura. Traction amplified actuation system for inspecting narrow and complex pipes using enhanced linear antagonistic mechanism-bend pipe passage model and force comparison. *IEEE Access*, 11:76156–76165, 2023.

[32] Jiankun Wang, Weinan Chen, Xiao Xiao, Yangxin Xu, Chenming Li, Xiao Jia, and Max Q-H Meng. A survey of the development of biomimetic intelligence and robotics. *Biomimetic Intelligence and Robotics*, 1:100001, 2021.

[33] Danying Sun, Jingyu Zhang, Qin Fang, Pingyu Xiang, Yanan Xue, Yue Wang, Rong Xiong, and Haojian Lu. Analysis and control for a bioinspired multi-legged soft robot. *Biomimetic Intelligence and Robotics*, 2(1):100030, 2022.

[34] Yanhong Peng, Hiroyuki Nabae, Yuki Funabora, and Koichi Suzumori. Controlling a peristaltic robot inspired by inchworms. *Biomimetic Intelligence and Robotics*, 4(1):100146, 2024.

[35] Hans Winkler and David A. Christie. Family picidae (woodpeckers). In J. del Hoyo, A. Elliot, and J. Sargatal, editors, *Handbook of the Birds of the World. Volume 7: Jacamars to Woodpeckers*. Lynx Edicions, 2002.

[36] Giacomo Mantriota and Arcangelo Messina. Theoretical and experimental study of the performance of flat suction cups in the presence of tangential loads. *Mechanism and machine theory*, 46(5):607–617, 2011.